ARTICLE IN PRESS

Available online at www.sciencedirect.com

SCIENCE DIRECT

ELSEVIER

Control Engineering Practice ▮ (▮▮▮▮) ▮▮▮–▮▮▮

CONTROL ENGINEERING PRACTICE

www.elsevier.com/locate/conengprac

Depth control of the INFANTE AUV using gain-scheduled reduced order output feedback ☆

C. Silvestre*, A. Pascoal

Instituto Superior Técnico, Institute for Systems and Robotics, Torre Norte - Piso 8, Av. Rovisco Pais 1 1046-001 Lisboa, Portugal

Received 21 October 2005; received in revised form 17 May 2006; accepted 23 May 2006

Abstract

The paper addresses the problem of autonomous underwater vehicle (AUV) control in the absence of full state information. An application is made to the control of a prototype AUV in the vertical plane. The methodology adopted for controller design is nonlinear gain-scheduling control, whereby a set of *linear*, *dynamic*, *reduced order output feedback controllers* are designed and scheduled on the vehicle's forward speed. The paper summarizes the controller design steps, describes a technique for its practical implementation, and presents experimental results obtained with the INFANTE AUV during tests at sea.

Keywords: Marine systems; Autonomous underwater vehicles; Gain-scheduled control; Output feedback; Linear matrix inequalities

1. Introduction

This paper describes a solution to the problem of autonomous underwater vehicle (AUV) control in the vertical plane, in the absence of full state information. An application is made to the control of the prototype INFANTE AUV, built and operated by the Instituto Superior Técnico of Lisbon, Portugal.

The paper starts by introducing a nonlinear dynamic model of the INFANTE AUV shown in Fig. 1. This is followed by control system design for precise maneuvering in the vertical plane. The technique adopted for controller design is gain scheduling (Rugh & Shamma, 2000). Using this approach, a set of linear controllers is first derived for a finite number of linearized models of the plant at selected operating points. The resulting controllers are then interpolated on the vehicle's forward speed.

For linear control system design, the paper exploits the use of reduced order feedback (ROF) techniques, which lead naturally to dynamic output feedback control laws with a very simple structure. In fact, the resulting controllers exhibit only the dynamics introduced by appended integrators (aimed at reducing steady-state tracking errors to zero) as well as extra dynamics that act as shaping filters to limit the actuation bandwidth. The importance of output feedback control strategies cannot be overemphasized: in practice, it is often impossible, difficult, or too expensive to measure the full state vector of a given plant. This motivates the development of controllers that rely on output variables only, effectively increasing the simplicity and thus the reliability of the control laws adopted. In the case of the INFANTE AUV, for example, it is difficult measure the angle of attack in the vertical plane. However, it is crucial to achieve stabilization and good maneuvering performance in that plane. This justifies the use of output feedback control techniques to meet desired stability and performance criteria.

From a theoretical point of view, the reduced order output feedback control problem can be converted into a static output feedback (SOF) problem for a related augmented system (Mäkilä, 1985). However, in spite of the availability of necessary and sufficient conditions for plant stabilizability by SOF, "no algorithm is currently available which guarantees to compute a stabilizing gain or

☆This work was supported by the Portuguese FCT POSI programme under framework QCA III, projects MAYA of the AdI and MAROV of the PDCTM, and by the EU under the FREESUB Network.

*Corresponding author. Tel.: +351218418052; fax: +351218418291.

E-mail addresses: cjs@isr.ist.utl.pt (C. Silvestre), antonio@isr.ist.utl.pt (A. Pascoal).

0967-0661/$ - see front matter © 2006 Elsevier Ltd. All rights reserved.
doi:10.1016/j.conengprac.2006.05.005

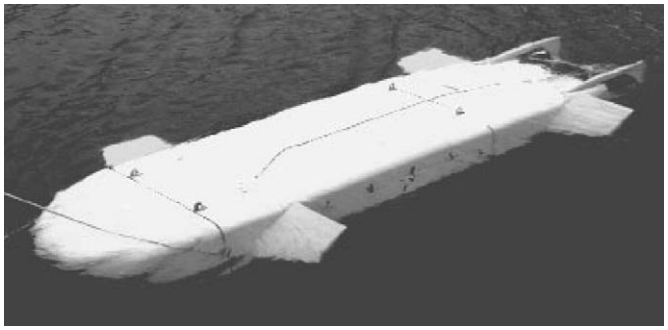

Fig. 1. The INFANTE vehicle.

determine if such a gain exists'' (Iwasaki, Skelton, & Geromel, 1994). The work in this area is well rooted in the theory of linear matrix inequalities (LMIs), which are steadily becoming the tool par excellence for advanced control system design. In fact, many control problems can be cast as LMI problems that can be solved efficiently using convex programming techniques. However, difficulties arise when designing (sub-optimal) SOF controllers because this problem can only be cast in terms of an equivalent one that involves bilinear matrix inequalities (BMIs) (Grigoriadis & Skelton, 1996). Because the resulting problem is no longer convex, no efficient numerical procedures exist for its solution as in the case of LMIs. However, the bilinear characteristics of the problem can still be exploited to derive an iterative procedure whereby two sets of LMIs are solved sequentially. This motivated the approach pursued in this paper, where the results described in (El Ghaoui, Oustry, & AitRami, 1997) are used to develop a simple algorithm to iteratively search for the solution to (sub-optimal) SOF control problems. Indirectly, the algorithm yields also a computational procedure to solve the ROF problem studied in this paper by exploiting the relationship between ROF and SOF control design techniques described in Mäkilä (1985). Although the algorithm performs a local search with no guarantees of global convergence, it exhibits excellent performance in the current application. See Leibfritz (2001) for a presentation of different techniques for the design of SOF controllers.

For the more theoretically oriented reader it is important to point out that in spite of tremendous progress in the area, the problems of designing fixed structure or fixed order controllers for a given plant are essentially open and continue to motivate active topics of research. A quick survey of recent publications is sufficient to show the reader how vibrant the area is. Nonsmooth optimization techniques that can be used to solve controller synthesis problems under additional structural constraints are presented in Apkarian and Noll (2006). In Kharitonov, Niculescu, Moreno, and Michiels (2005), the authors give necessary conditions for the existence of SOF stabilization controllers for a class of single-input–single-output systems when the control law includes multiple (distinct) delays; illustrative examples that include a second-order systems, and chains of integrators are presented and discussed. In Henrion and Lasserre (2006), the authors propose a hierarchy of convex linear matrix inequality relaxations using a moment interpretation of recent results on sum-of-squares decompositions of nonnegative polynomial matrices to solve nonconvex polynomial matrix inequality (PMI) optimization problems. The latter include BMIs, the solution of which yields efficient techniques for the computation of ROF $\mathbf{H}_2$ or $\mathbf{H}_\infty$ controllers. A sufficient condition for the SOF stabilization of linear discrete-time systems expressed as an LMI feasibility problem is presented in Bara and Boutayeb (2005), where the authors validate the applicability of the algorithms proposed through numerical examples. Finally, an application of an (LMI)-based procedure for the design of robust SOF controllers is presented in Benton and Smith (2005), where a solution to the emergency lateral control problem of a highway vehicle with bounded time-varying uncertainties is presented and discussed. In the paper, a stabilizing SOF controller is designed and its gains are reduced while guaranteeing robust stability.

In the work reported here, a finite number of ROF controllers were developed for linearized plant models obtained at different operating conditions determined by the vehicle's forward speed. The controller parameters were then interpolated and scheduled on speed (that is, dynamic pressure). The final implementation of the resulting nonlinear gain-scheduled controller was done using the D-methodology described in Kaminer, Pascoal, Khargonekar, and Coleman (1995) that guarantees a fundamental linearization property and avoids the need to feedforward the values of the state variables and inputs at trimming.

The paper is organized as follows. Section 2 introduces a nonlinear model for the vertical plane dynamics of the INFANTE AUV. Section 3 details the techniques that were used for depth control system design and implementation. Finally, Section 4 contains experimental results obtained during sea trials of the vehicle in the Azores, Portugal. Section 5 contains the main conclusions and describes related problems that warrant future research.

2. Vehicle dynamics

This section describes the dynamic model of the INFANTE AUV in the vertical plane. See Silvestre (2000) for details. The vehicle is 4.5 m long, 1.1 m wide and 0.6 m high. It is equipped with two main thrusters (propellers and nozzles) for cruising and fully moving surfaces (rudders, bow planes and stern planes) for vehicle steering and diving in the horizontal and vertical planes, respectively. The maximum rated speed of the vehicle with respect to the water will not exceed 3.5 m/s.

The notation used in the paper and the structure of the vehicle model are standard (Fossen (1994); Silvestre (2000)). The variables u and w denote surge and heave speeds, respectively, while θ, q, and z denote pitch, pitch rate and depth. The vector $\boldsymbol{\delta} = [\delta_b, \delta_s]'$ consists of bow and

stern plane deflections δ_b and δ_s, respectively. With this notation, and neglecting the roll stable motion, the dynamics of the AUV in the vertical plane can be written in compact form as

Dynamics:

$$M_{RB}\ddot{\mathbf{q}} + C_{RB}(\dot{\mathbf{q}})\dot{\mathbf{q}} = \boldsymbol{\tau}(\ddot{\mathbf{q}}, \dot{\mathbf{q}}, \boldsymbol{\delta}, n), \tag{1}$$

$$\dot{\mathbf{q}} = [u, w, q]'. \tag{2}$$

Kinematics:

$$\frac{\mathrm{d}}{\mathrm{d}t}[x, z]' = R(\theta)[u, w]', \tag{3}$$

$$\dot{\theta} = q, \tag{4}$$

where $[x, z]'$ is the position of the vehicle's center of mass, $R(\theta)$ is the rotation matrix from body to inertial coordinate frame parameterized by pitch angle θ, and $\boldsymbol{\tau}$ denotes the vector of external forces and torques acting on the vehicle. The symbols M_{RB} and C_{RB} denote the rigid body inertia matrix and the matrix of Coriolis and centripetal terms, respectively, see Fossen (1994) and Silvestre (2000) for further details.

The vector $\boldsymbol{\tau}$ can further be decomposed as

$$\boldsymbol{\tau}(\ddot{\mathbf{q}}, \dot{\mathbf{q}}, \boldsymbol{\delta}, n) = \boldsymbol{\tau}_{add}(\ddot{\mathbf{q}}, \dot{\mathbf{q}}) + \boldsymbol{\tau}_{surf}(\dot{\mathbf{q}}, \boldsymbol{\delta}) + \boldsymbol{\tau}_{body}(\dot{\mathbf{q}}, \boldsymbol{\delta}) + \boldsymbol{\tau}_{prop}(\dot{\mathbf{q}}, n), \tag{5}$$

where $\boldsymbol{\tau}_{add}$ represents the added mass effects. The term $\boldsymbol{\tau}_{surf}$ captures the effects of deflections of the control surfaces, $\boldsymbol{\tau}_{body}$ consists of the hydrodynamic forces and torques acting on the vehicle's body, and $\boldsymbol{\tau}_{prop}$ represents the forces and torques due to the main propellers.

2.1. System identification. Hydrodynamic tank tests

To be of practical use, the model described by Eqs. (1)–(4) must be tuned for the particular vehicle in study. Clearly, the main difficulty lies in computing the term $\boldsymbol{\tau}$ that arises in the dynamics equation. In the case of the INFANTE AUV, this was achieved by using a combination of theoretical methods and experimental data obtained previously for the MARIUS AUV (Egeskov et al., 1994).

The added mass term was estimated in part by assuming ellipsoidal and elliptical cylinder approximations for the body and control surfaces, respectively (Lamb, 1932; Newman, 1977). Approximations to the lift and drag terms of the control surfaces were obtained using thin airfoil theory. Additional terms were computed based on data determined from the following series of tank tests carried out at the Danish Maritime Institute (DMI) in Lyngby, Denmark for the MARIUS AUV:

(i) Open water tests of the propeller/nozzle system to determine its characteristics in undisturbed (open) water.
(ii) Resistance tests to measure the resistance of the vehicle without the propulsion system in place.
(iii) Self-propulsion tests to assess the performance of the propulsion system in the wake of the hull.
(iv) Planar Motion Mechanism tests in the horizontal and vertical planes to measure the most relevant hydrodynamic derivatives of the vehicle.

The reader is referred to Abkowitz (1964) and Harvald (1983) for an introduction to these standard tests. See also Egeskov et al. (1994) for the results of the tests in Denmark.

The rest of this section presents the most relevant vertical plane hydrodynamic derivatives of the INFANTE vehicle. These terms account for the interaction of the vehicle's hull and deflection surfaces with the surrounding fluid and capture the variation of the forces and torques experienced by the vehicle when it deviates from its normal cruising condition (moving forward along a straight line in the vertical plane). With a certain abuse of notation, the hydrodynamic derivatives can be viewed as resulting from a Taylor series expansion of the forces and torques about the nominal operating condition. In general, hydrodynamic derivatives are functions of the nominal vehicle's total speed (Abkowitz, 1964). In this paper, the normal procedure of replacing the vehicle's total speed by its forward speed u is adopted. This procedure is justified for the case when the vertical heave speed is small.

From Eqs. (1) and (5), using the standard SNAME notation (Fossen, 1994; Lewis, 1990), the hydrodynamic forces and torques in the vertical plane can be expressed as

$$[X_h,\ Z_h,\ M_h]' = \boldsymbol{\tau}(\ddot{\mathbf{q}}, \dot{\mathbf{q}}, \boldsymbol{\delta}, n),$$

where X_h and Z_h denote the forces along the vertical plane (x and z axis) and M_h is the torque about the y body axis. Expanding in terms of nondimensional hydrodynamic derivatives yields

Hydrodynamic forces:

$$X_h = \frac{\rho}{2}L^2[X_{uu}u^2 + X_{ww}w^2] + \frac{\rho}{2}L^2u^2[X_{\delta_b\delta_b}\delta_b^2 + X_{\delta_s\delta_s}\delta_s^2] + \frac{\rho}{2}L^4X_{qq}q^2 + \frac{\rho}{2}L^3X_{\dot{u}}\dot{u} + T, \tag{6}$$

$$Z_h = \frac{\rho}{2}L^2Z_wuw + \frac{\rho}{2}L^3Z_quq + \frac{\rho}{2}L^2u^2[Z_{\delta_b}\delta_b + Z_{\delta_s}\delta_s] + \frac{\rho}{2}L^3Z_{\dot{w}}\dot{w} + \frac{\rho}{2}L^4Z_{\dot{q}}\dot{q}, \tag{7}$$

$$M_h = \frac{\rho}{2}L^3M_wuw + \frac{\rho}{2}L^4M_quq + \frac{\rho}{2}L^3u^2[M_{\delta_b}\delta_b + M_{\delta_s}\delta_s] + \frac{\rho}{2}L^4M_{\dot{w}}\dot{w} + \frac{\rho}{2}L^5M_{\dot{q}}\dot{q}, \tag{8}$$

where T denotes the total longitudinal force imparted by the thrusters. The main particulars for the INFANTE vehicle in the vertical plane are $I_y = 1700\,\mathrm{Nm\,s^2}$, $m = 2234.5\,\mathrm{kg}$, $\rho = 1030\,\mathrm{kg/m^3}$, and $L = 4.22\,\mathrm{m}$. Table 1 lists the most relevant *nondimensional hydrodynamic derivatives* of the vehicle vertical plane model, following the standard notation of Lewis (1990). In the table, the hydrodynamic parameters are normalized using the

Table 1
Nondimensional hydrodynamic coefficients for the INFANTE AUV in the vertical plane—$\times 10^{-5}$

X		Z		M	
X_{uu}	−387				
$X_{\dot{u}}$	−368				
X_{ww}	−978	Z_w	−32805	M_w	5476
		$Z_{\dot{w}}$	−11973	$M_{\dot{w}}$	−1286
X_{qq}	5898	Z_q	6790	M_q	−3878
		$Z_{\dot{q}}$	−1047	$N_{\dot{q}}$	−247
$X_{\delta_b\delta_b}$	−4980	Z_{δ_b}	−7539	M_{δ_b}	2411
$X_{\delta_s\delta_s}$	−4980	Z_{δ_s}	−7539	M_{δ_s}	−2052

characteristic length L and the surface deflections are expressed in radians.

2.2. Control model

For control design purposes, the vehicle was assumed to be commanded directly in thrust T. In this case, the simplified vertical plane dynamics can be written in dimensional form as

Surge motion equation:

$$m\dot{u} = C_X u^2 + C_{X_{ww}} w^2 + C_{X_{qq}} q^2 + u^2 C_{X_{\delta_b\delta_b}} \delta_b^2 + u^2 C_{X_{\delta_s\delta_s}} \delta_s^2 + C_{X_{\dot{u}}} \dot{u} + T, \quad (9)$$

Heave motion equation:

$$m(\dot{w} - uq) = (W - B)\cos(\theta) + C_{Z_w} uw + C_{Z_q} uq + C_{Z_{\delta_b}} \delta_b + C_{Z_{\delta_s}} \delta_s + C_{Z_{\dot{w}}} \dot{w} + C_{Z_{\dot{q}}} \dot{q}, \quad (10)$$

$$\dot{z} = -u\sin(\theta) + w\cos(\theta), \quad (11)$$

Pitch motion equation:

$$I_y \dot{q} = z_{CB} B \sin(\theta) + C_{M_w} uw + C_{M_q} uq + C_{M_{\delta_b}} \delta_b + C_{M_{\delta_s}} \delta_s + C_{M_{\dot{w}}} \dot{w} + C_{M_{\dot{q}}} \dot{q}, \quad (12)$$

$$\dot{\theta} = q, \quad (13)$$

where Eqs. (9), (10) and (12) describe the surge, heave and pitch motion, respectively, and $C_{(.)}$ are the simplified model coefficients represented in Table 2.

It is important to point out that the type of experimental data obtained in the course of the PMM tests, as well as the computation of some of the vehicle parameters using thin airfoil theory limit the regions of validity of the horizontal and vertical submodel described above. In fact, the model derived is only valid for small angles of attack, and for small control surface deflections (Abkowitz, 1964). In practice these limitations are not severe, since they represent the normal operating conditions of a vehicle with the shape of the INFANTE AUV.

To develop a depth controller, the vehicle's forward nominal speed $u = u_0$ is assumed to be constant and the

Table 2
Dimensional hydrodynamic coefficients for the INFANTE AUV in the vertical plane: surge, heave and pitch motions

$C_{X_{\dot{u}}} = \frac{1}{2}\rho X_{\dot{u}} L^3$,	$C_X = \frac{1}{2}\rho X_{uu} L^2$,
$C_{X_{ww}} = \frac{1}{2}\rho X_{ww} L^2$,	$C_{X_{qq}} = \frac{1}{2}\rho X_{qq} L^4$,
$C_{X_{\delta_b\delta_b}} = \frac{1}{2}\rho X_{\delta_b\delta_b} L^2$,	$C_{X_{\delta_s\delta_s}} = \frac{1}{2}\rho X_{\delta_s\delta_s} L^2$,
$C_{Z_{\dot{w}}} = \frac{1}{2}\rho Z_{\dot{w}} L^3$,	$C_{Z_w} = \frac{1}{2}\rho Z_w L^2$,
$C_{Z_{\dot{q}}} = \frac{1}{2}\rho Z_{\dot{q}} L^4$,	$C_{Z_q} = \frac{1}{2}\rho Z_q L^3$,
$C_{Z_{\delta_b}} = \frac{1}{2}\rho Z_{\delta_b} L^2$,	$C_{Z_{\delta_s}} = \frac{1}{2}\rho Z_{\delta_s} L^2$,
$C_{M_{\dot{w}}} = \frac{1}{2}\rho M_{\dot{w}} L^4$,	$C_{M_w} = \frac{1}{2}\rho M_w L^3$,
$C_{M_{\dot{q}}} = \frac{1}{2}\rho M_{\dot{q}} L^5$,	$C_{M_q} = \frac{1}{2}\rho M_q L^4$,
$C_{M_{\delta_b}} = \frac{1}{2}\rho M_{\delta_b} L^3$,	$C_{M_{\delta_s}} = \frac{1}{2}\rho M_{\delta_s} L^3$

vertical plane model is formally written as

$$\frac{\mathrm{d}}{\mathrm{d}t}\mathbf{x}_v = F_v(\mathbf{x}_v, \mathbf{u}_v), \quad (14)$$

where $\mathbf{x}_v = [w, q, \theta]' \in \mathbb{R}^3$ is the state vector, $\mathbf{u}_v = [\delta_b, \delta_s]' \in \mathbb{R}^2$ is the input vector, and $F_v : \mathbb{R}^3 \times \mathbb{R}^2 \to \mathbb{R}^3$ is a nonlinear function that is easily obtained from the surge, and pitch equations of motion, together with the kinematic depth and pitch relationships described by Eqs. (11) and (13).

3. Control system design and implementation

This section describes the design of a depth control system for the AUV INFANTE, based on the dynamic model presented in Section 2. The methodology adopted for controller design is nonlinear gain-scheduled control, whereby the design of a controller to achieve stabilization and adequate performance of a given nonlinear plant (system to be controlled) involves the following steps (Rugh & Shamma, 2000):

(i) *Linearizing* the plant about a finite number of representative operating points,
(ii) Designing *linear controllers* for the plant linearizations at each operating point,
(iii) *Interpolating* the parameters of the linear controllers of Step (ii) to achieve adequate performance of the linearized closed-loop systems at all points where the plant is expected to operate. The interpolation is performed according to an external scheduling variable (vehicle's forward speed), and the resulting family of linear controllers is referred to as a *gain-scheduled controller*,
(iv) *Implementing* the gain-scheduled controller on the original nonlinear plant.

In what follows a brief summary is given of the work done at each of the design steps, leading to the development of a controller for the vehicle that is scheduled on forward speed. For the sake of brevity, the linear design methodology is illustrated for the case of a single operating condition that corresponds to a forward speed of 2.0 m/s.

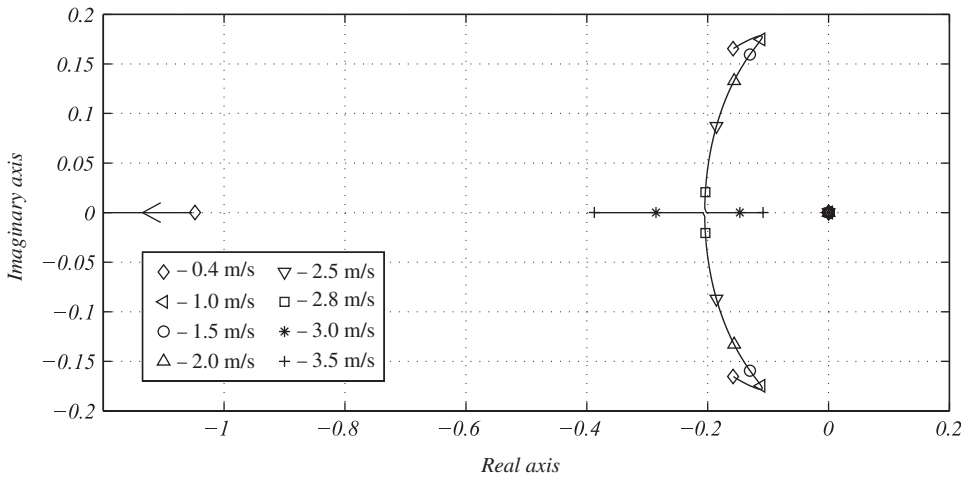

Fig. 2. Linearized model eigenvalues as functions of the forward speed u_0.

Linearization. open-loop system analysis: The model for the vertical plane was linearized about the equilibrium point determined by $[w_0, q_0, z_0, \theta_0]' = [0, 0, 0, 0]'$ and $\mathbf{u}_0 = [\delta_b, \delta_s]' = [0, 0]'$.

The resulting linearized model eigenvalues are presented in Fig. 2. The model exhibits an eigenvalue at zero (corresponding to a pure integrator in the depth coordinate z) and three *stable* eigenvalues that link together the variables w, q and θ. Notice the overall trend in the plot, where the two complex eigenvalues at low speed degenerate into two real eigenvalues at higher speed. The state space linearized dynamics and input matrices for the forward velocity of 2.0 m/s are represented below:

$$A = \begin{bmatrix} -1.400 & 2.763 & 0.0 & 0.078 \\ 2.108 & -5.419 & 0.0 & -0.312 \\ 1.0 & 0.0 & 0.0 & -2.0 \\ 0.0 & 1.0 & 0.0 & 0.0 \end{bmatrix},$$

$$B = \begin{bmatrix} -0.797 & -0.201 \\ 1.588 & -0.809 \\ 0.0 & 0.0 \\ 0.0 & 0.0 \end{bmatrix}.$$

The state space matrix A has one second-order mode with a natural frequency of 0.121 rad/s, a real eigenvalue at -6.5 rad/s, and a zero eigenvalue. Notice that the variable θ does not exhibit a pure integration effect, due to the existence of a restoring torque caused by the combined effect of buoyancy and gravity. In the input matrix, the bow and stern plane deflections δ_b and δ_s affect directly the state variables w and q.

3.1. Design specifications

The linear depth controllers were required to meet the following design specifications:

Zero steady-state error: Achieve zero steady-state values for the error variable in response to the input commands z_{cmd}.

Bandwidth requirements: The input–output command response bandwidth for the depth command channel should be on the order of 0.1 rad/s; the control loop bandwidth for the bow and stern planes channels should not exceed 5 rad/s; these figures were selected to ensure that the actuators would not be driven beyond their normal actuation bandwidth.

Closed-loop damping and stability margins: The closed-loop eigenvalues should have a damping ratio of at least 0.7 and a real part of at most -0.1 rad/s. It was also required that the steady-state deflection of the bow planes in response to a step input command in depth be $\delta_b = 0$.

3.2. Brief theoretical background

The methodology selected for linear control system design was reduced order output feedback with an $\mathbf{H}_\infty$ criterion (Grigoriadis & Skelton, 1996). This method rests on a firm theoretical basis and leads naturally to an interpretation of control design specifications in the frequency domain. Furthermore, it provides clear guidelines for the design of controllers so as to achieve robust performance in the presence of plant uncertainty.

The design tools adopted are LMIs, which are steadily becoming a standard tool for the design of advanced control systems. See Boyd, El Ghaoui, Feron, and Balakrishnan (1994) for a lucid exposition of the subject and an historical perspective. As explained in Boyd et al. (1994) and El Ghaoui and Niculescu (1999), the story of LMIs can be traced back to the work of Lyapunov, who showed that the origin of the linear time-invariant system $\mathrm{d}x(t)/\mathrm{d}t = Ax(t)$ is asymptotically stable if and only if there exists a positive definite matrix P such that $A'P + PA < 0$. Let $P_1, P_2, \ldots, P_m$ be a basis for the space of nxn positive definite matrices, with $m = n \times (n+1)/2$. Further let $F_0 = 0$ and $F_i = A'P + P_iA$. Then, finding P

positive definite that satisfies the equation above (or determining that none exists) is equivalent to determining whether a vector $\mathbf{x} = (x_1, \ldots, x_n)' \in \mathbb{R}^n$ exists such that

$$F(\mathbf{x}) = F_0 + \sum_{i=1}^{n} x_i F_i < 0 \tag{15}$$

is satisfied.

An LMI is any constraint $F(\mathbf{x})$ of the form introduced above. In the general case, the vector $\mathbf{x} = (x_1, \ldots, x_n)' \in \mathbb{R}^n$ represents the free design variables (also called decision variables) and the symmetric matrices $F_i = F_i' \in \mathbb{R}^{n \times n}$ are given. The inequality symbol in Eq. (15) means that $F(\mathbf{x})$ is negative definite, i.e., for all nonzero $u \in \mathbb{R}^n$, $u'F(\mathbf{x})u < 0$. Solving this inequality consists of finding $\mathbf{x}$ such that (15) holds.

LMIs present the following appealing property for computational purposes: finding a feasible $\mathbf{x}$ such that $F(\mathbf{x}) < 0$ is a convex optimization problem for which efficient interior point algorithms have been developed and implemented in the Matlab LMI Toolbox.

In general, multiobjective/multicriteria control problems, where mixed time and frequency domain specifications must be met, are extremely difficult to solve. However, within the LMI framework, multiobjective/multicriteria problems involving simultaneous $\mathbf{H}_2$ and $\mathbf{H}_\infty$ performance criteria as well as regional eigenvalue placement, settling time, saturation, and initial conditions response specifications, can be formulated and solved using advanced numerical tools. The key idea in the LMI approach to multiobjective/multicriteria controller design consists of converting each closed-loop control objective or specification into an additional constraint on the class of admissible closed-loop Lyapunov functions. This design technique expresses the desired closed-loop control objectives and specifications in terms of a set of LMIs (involving a single Lyapunov function) which, if feasible, guarantee simultaneous achievement of the different closed-loop requirements, possibly at the expense of being conservative.

In summary, LMIs provide a powerful formulation as well as a versatile design technique for a wide variety of linear control problems. Since solving LMIs is a convex optimization problem for which numerical solvers are now available, reducing a control problem to an LMI can be seen as a practical solution for many control problems.

3.3. Linear control system design

The reduced order output feedback (ROF) control problem can be solved by converting it into a SOF control problem, using a well-known system augmentation technique (El Ghaoui et al., 1997). To this effect, consider the original plant dynamics $\Sigma_m = \{A_m, B_m, C_m\}$ and the appended dynamics $\Sigma_k = \{A_k = 0_k, B_k = I_k, C_k = I_k\}$ of order k. Let $\mathbf{u}_k \in \mathbb{R}^k$, and $\mathbf{x}_k \in \mathbb{R}^k$, be the control input and state of the appended dynamics. It can be shown (Mäkilä, 1985) that the ROF stabilization problem has a solution of order k if and only if the augmented system

$$A = \begin{bmatrix} A_k & 0 \\ 0 & A_m \end{bmatrix}, \quad B = \begin{bmatrix} B_k & 0 \\ 0 & B_m \end{bmatrix}, \quad C = \begin{bmatrix} C_k & 0 \\ 0 & C_m \end{bmatrix}$$

admits a SOF stabilizing solution. Therefore, solving the SOF problem for the augmented system is equivalent to solving the reduced order output feedback problem for the original plant. In other words, given a reduced order controller design problem—where the problem data consist of a nominal plant model and a set of H-infinity performance specifications associated with the plant states and inputs—there is an equivalent static output feedback control problem for an augmented plant that can be cast in terms of the feasibility of a set of LMIs. If the latter are feasible, then their solution will yield directly an output feedback controller for the augmented plant and, indirectly, a reduced order output feedback controller for the original plant. The remainder of this section focuses on the SOF problem.

In what follows, the standard setup and nomenclature in Zhou, Doyle, and Glover (1995) is adopted, leading to the feedback system represented in Fig. 3 with realization

$$\begin{cases} \dot{\mathbf{x}}(t) = A\mathbf{x}(t) + B_w\mathbf{w}(t) + B\mathbf{u}(t), \\ \mathbf{z}(t) = C_z\mathbf{x}(t) + D\mathbf{w}(t) + E\mathbf{u}(t), \quad \mathbf{u}(t) = K\mathbf{y}(t), \\ \mathbf{y}(t) = C\mathbf{x}(t) + F\mathbf{w}(t), \end{cases} \tag{16}$$

where $\mathbf{x}$ is the state vector. The symbol $\mathbf{w}$ denotes the input vector of exogenous signals (including commands and disturbances), $\mathbf{z}$ is the output vector of errors to be reduced, $\mathbf{y}$ is the vector of measurements that are available for feedback, and $\mathbf{u}$ is the vector of actuator signals. The generalized plant G consists of the augmented system described before together with weights that shape the exogenous and internal signals, see Section 3.4. Suppose that the feedback system is well-posed, and let $T_{\mathbf{zw}}$ denote the closed-loop operator from $\mathbf{w}$ to $\mathbf{z}$. The (sub-optimal) $\mathbf{H}_\infty$ SOF synthesis problem consists of finding (if it exists) a static controller K that stabilizes the closed-loop system and makes the infinity norm $\|\mathrm{T}_{\mathbf{zw}}\|_\infty$ of the operator $\mathrm{T}_{\mathbf{zw}}$ smaller than a desired bound $\gamma > 0$.

Let $A_{cl} = (A + BKC)$ be the closed-loop system matrix of (16) with K to be determined. The technique used for controller design is based on the following standard results

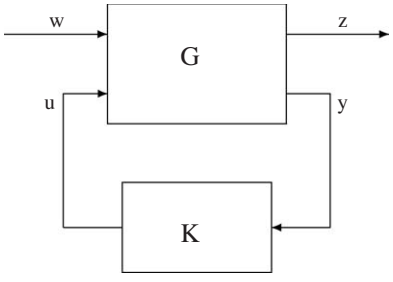

Fig. 3. Feedback interconnection.

(Chilali & Gahinet, 1996; El Ghaoui & Niculescu, 1999; Zhou et al., 1995).

Result 1: The closed-loop system with realization (16) has all the eigenvalues in the semi-plane $\lambda \in C$: $\mathrm{Re}(\lambda) < -\alpha$ if a real symmetric matrix $X > 0$ exists such that the closed-loop Lyapunov inequality

$$X(A_{cl}' + \alpha I) + (A_{cl} + \alpha I)X < 0 \tag{17}$$

is satisfied.

Result 2: The $\mathbf{H}_\infty$ norm of the operator $T_{\mathbf{zw}}$ is less than a positive number γ, that is, $\|T_{\mathbf{zw}}\|_\infty < \gamma$, if a real symmetric matrix $X > 0$ exists such that the LMI

$$\begin{bmatrix} XA_{cl}' + A_{cl}X & * & * \\ B_w' & -\gamma I & * \\ C_z X + EKC & D & -\gamma I \end{bmatrix} < 0 \tag{18}$$

holds.

Additional closed-loop regional eigenvalues placement specifications can also be converted into design constraints by using the concept of LMI regions in the complex plane, as introduced by Chilali and Gahinet (1996), thus generalizing Result 1. Let $L = [l_{ij}]$ and $M = [m_{ij}]$ be real symmetric matrices. An LMI region R_{lmi} is defined as an open domain in the complex plane that satisfies

$$\mathrm{R}_{lmi} = \{z \in \mathbf{C} : l_{ij} + m_{ij} z + m_{ji} \bar{z} < 0; \quad i,j = 1,\ldots,n\}. \tag{19}$$

This description can represent a large number of regions which are symmetric with respect to the real axis, such as conic sectors, half-planes, etc. Using the concept of LMI regions, Result 1 admits the following generalization, see Chilali and Gahinet (1996) for further details:

Result 3: The closed-loop system with realization (16) has all the eigenvalues in the region R_{cl} defined by (19) if a real symmetric matrix $X > 0$ exists such that the closed-loop generalized Lyapunov inequality

$$l_{ij}X + m_{ij}A_{cl}X + m_{ji}XA_{cl}' < 0, \quad i,j = 1,\ldots,n. \tag{20}$$

is satisfied.

In the present design case, the closed-loop eigenvalues are required to lie in the region depicted in Fig. 4. Simple computations show that in this case (20) degenerates into

$$\begin{bmatrix} \sin(\theta_{reg})(A_{cl}X + XA_{cl}') & \cos(\theta_{reg})(XA_{cl}' - A_{cl}X) & 0 \\ \cos(\theta_{reg})(A_{cl}X - XA_{cl}') & \sin(\theta_{reg})(A_{cl}X + XA_{cl}') & 0 \\ 0 & 0 & A_{cl}X + XA_{cl}' + 2\alpha_{reg}X \end{bmatrix} < 0, \tag{21}$$

where the parameters α_{reg} and θ_{reg} were set to $\alpha_{cl} = -0.1$ and $\theta_{cl} = 45^\circ$, respectively, so as to meet the desired closed-loop performance specifications.

In the case of a square full rank matrix C, the standard transformation $W = KCX$ converts the above nonlinear LMIs into convex LMIs. However, in the case of a noninvertible C matrix, the problem of determining a sub-optimal SOF controller involves solving BMIs. In this situation, the problem at hand is no longer convex, thus

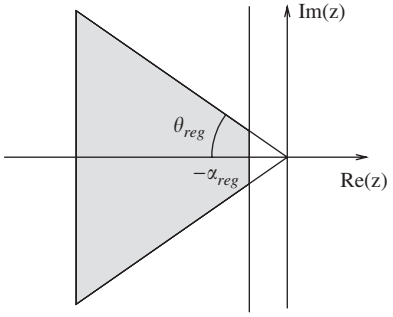

Fig. 4. A typical closed loop generalized stability region.

making the task of finding numerical solutions hard. It is relevant to point out that given an arbitrary dynamic system, there are no guarantees that a SOF controller exists that will stabilize the system. Furthermore, even if the existence of a stabilizing controller can be established, the nonconvex characteristics of the optimization problem are such that no assurances can be given as to whether a numerical procedure will converge to a solution. Therefore, the following algorithms for the computation of a sub-optimal $\mathbf{H}_\infty$ SOF controller should only be adopted if sound judgement is applied to establish if a solution to the (sub-optimal) $\mathbf{H}_\infty$ SOF synthesis problem can indeed be found.

The algorithms proposed for control system design can be briefly explained as follows: (i) compute (if it exists) a SOF stabilizing controller for the generalized plant G, and (ii) use this controller as a starting point to find an $\mathbf{H}_\infty$ sub-optimal controller, subject to regional eigenvalue placement constraints. Algorithm 1 finds a stabilizing controller using Result 1, starting with an arbitrary K of appropriate dimensions.

Algorithm 1 (*SOF stabilizing controller*).

(1) For an arbitrary K find α such that $Re(\lambda_i(A + \alpha I)) < 0$, $i = 1,\ldots,n$.
(2) Fix K and solve LMI (17) (feasibility problem) with respect to variable X.
(3) Fix X and solve the optimization problem of minimizing α subject to the LMI constraint (17) in the variables α, and K.
(4) If $\alpha \leqslant \alpha_{cl}$ go to step 1, else end.

The second algorithm computes a SOF $\mathbf{H}_\infty$ sub-optimal controller using Result 2, adopting the stabilizing static controller K obtained before as a starting point.

Algorithm 2 (*SOF* $\mathbf{H}_\infty$ *sub-optimal controller with regional pole placement constraints*).

(1) Set $\theta_{reg} = 90^\circ$, $\alpha_{reg} = \alpha_{cl}$.
(2) Fix K and solve the optimization problem of minimizing γ subject to the LMI constraints (18) and (21) in the variables γ and X. Set $\gamma_1 = \gamma$ found.
(3) Fix X and solve the optimization problem of minimizing γ subject to the LMI constraint (18) and (21) in the variables γ and K. Set $\gamma_2 = \gamma$ found.
(4) If $\theta_{reg} < \theta_{cl}$, set $\theta_{reg} = \theta_{cl}$.
(5) If $|\gamma_1 - \gamma_2| > \zeta$ or $\theta_{reg} > \theta_{cl}$ go to step 2, else end.

In this design exercise, ζ was set to 0.001.

Finally, the ROF controller is computed from the augmented system and the gain K.

3.4. Synthesis model and controller design

The first step in the controller design procedure is the development of a synthesis model that can serve as an interface between the designer and the $\mathbf{H}_\infty$ controller synthesis algorithm.

Consider the feedback system shown in Fig. 5, where P is the augmented linearized model of the AUV in the vertical plane (including the Σ_k dynamics), and K is a SOF controller to be designed. The block G within the dashed line is the synthesis model, which is derived from the linear augmented model of the plant by appending the depicted weights. In practice, the weights serve as tuning "knobs" which the designer can adjust to meet the desired performance specifications.

In the figure, $\mathbf{w}_1$ represents the depth command z_{cmd} that must be tracked. The vector $\mathbf{w}_2$ includes the input noise to each of the sensors that provide measurements of depth, pitch and pitch rate as well as disturbance inputs to the states w and q of the plant. The signal $\mathbf{u}$ represents the augmented system control inputs that consist of $\mathbf{u}_k$ and the bow and stern plane deflections δ_b, and δ_s, respectively, and vector $\mathbf{e} = \mathbf{w}_1 - \mathbf{x}_1$ is the respective depth tracking error. The signal $\mathbf{x}_2$ contains the remaining state variables that must be penalized in the design process, that is, w, q and θ. The matrices W_i; $i = 1, \ldots, 4$ correspond to dynamic weights that penalize input, state and tracking variables. Finally, the signal $\mathbf{y}$ consists of variables $\mathbf{x}_k$, q, θ, z, $\mathbf{e}/s$ and δ_b/s that are available for feedback. To meet the depth step command response requirement the weighting function W_1 was chosen as $W_1 = 0.1$. The weight W_2 on the actuation vector $\mathbf{u}$ was selected as $W_2 = \mathrm{diag}(0.5, 0.5, W_a(s))$. Block $W_a(s)$ is a dynamic weight matrix used to enforce the bandwidth constraint on the bow and stern planes, as discussed later. The weight W_3 was set to $\mathrm{diag}(22.0, 0.1, 0.01, 0.05, 0.05)$ to meet the command bandwidth requirements, and $W_4 = 0.001 I_4$. Notice the existence of a block of integrators I/s that operates on the tracking errors $\mathbf{e}$ and on the entries of the control input vector $\mathbf{u}$ that are selected by the matrix S. Integral action on the errors is required to ensure zero steady state in response to step commands in $\mathbf{w}_1$. Integral action on the entries of $\mathbf{u}$ introduces a "washout" on the particular control inputs selected. In the present case, the "washout" ensures zero bow plane deflection at trimming conditions.

The constraints on the maximum bow and stern plane actuation bandwidths were converted into a $\mathbf{H}_\infty$ design specification through the operator $W_a(s)$ using the appended (nonobservable from $\mathbf{y}$) stable dynamic weight shown in Fig. 6.

In the figure, vector $\mathbf{z}_a$ (which during the design process is included in the overall performance vector $\mathbf{z}$) represents the bow and stern plane actuation channels after being weighted by two first-order linear stable transfer functions. For the case studied in this paper, the matrix operator $W_a(s)$ was set to

$$W_a(s) = 2\begin{bmatrix} \dfrac{s/6+1}{(s/30+1)} & 0 \\ 0 & \dfrac{s/6+1}{(s/30+1)} \end{bmatrix}.$$

The inclusion of these high-pass weights expedites the process of fine tuning the closed-loop bandwidths of the control planes because it penalizes high-frequency components of the actuation signals. After several iterations the controller order was set to $k = 2$ to accommodate the

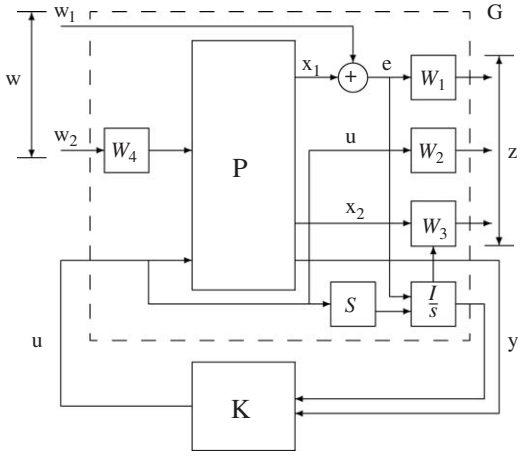

Fig. 5. Synthesis model.

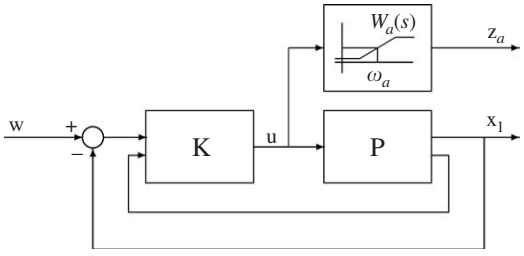

Fig. 6. Actuators bandwidth constraint.

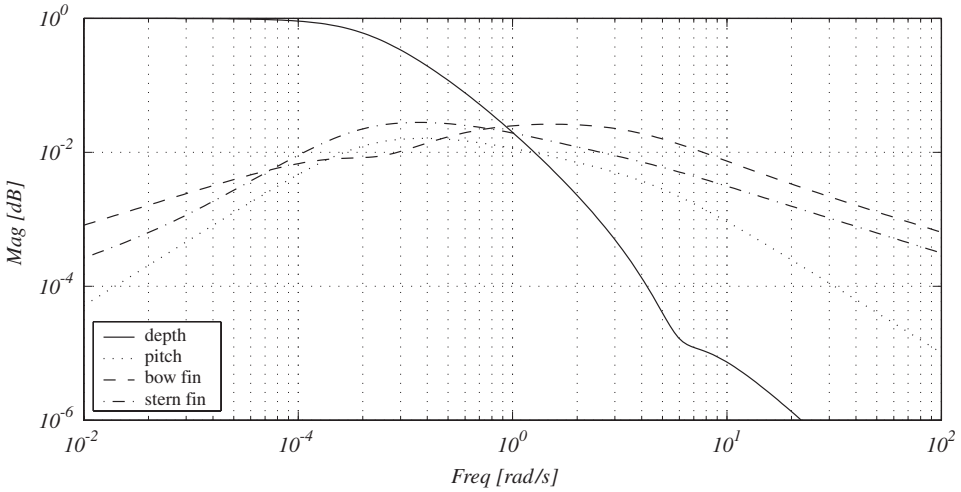

Fig. 7. Closed-loop frequency responses.

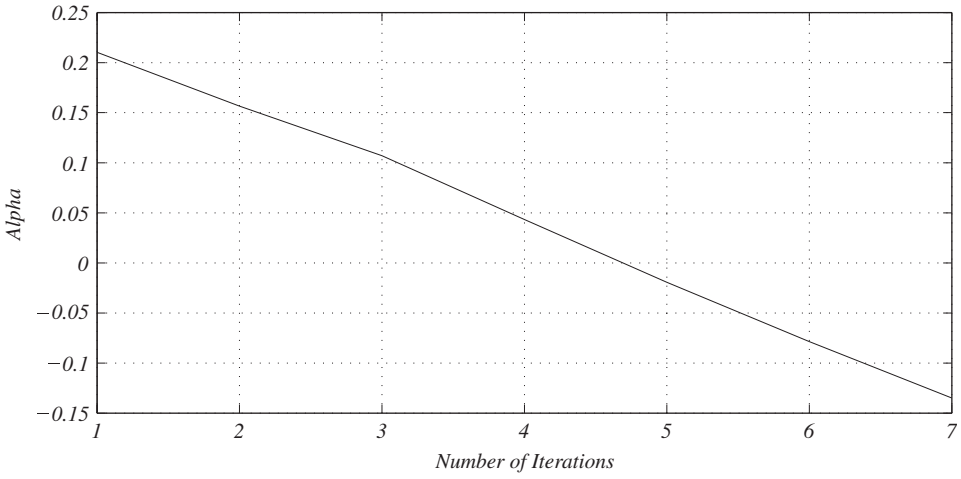

Fig. 8. Evolution of α.

required actuator bandwidth constraints and the order of the resulting ROF controller was 4.

Fig. 7 shows the Bode diagrams for the closed-loop transfer functions from the depth command input z_{cmd} to the variables z, θ, δ_s and δ_b for the 2.0 m/s controller. The diagram shows that the performance requirements and the actuator bandwidth constraints are met by the resultant closed-loop system.

Figs. 8 and 9 illustrate the efficacy of the controller synthesis technique proposed. Fig. 8 shows the evolution of variable α during the first phase of the controller synthesis (Algorithm 1). Fig. 9 depicts the evolution of γ, the $\mathbf{H}_\infty$ norm of the system under study (second phase, Algorithm 2) for the 2.0 m/s controller. Notice that in this case the overall controller synthesis procedure requires seven iterations to find a stabilizing controller and 68 iterations to compute the sub-optimal reduced order output feedback controller. The regional eigenvalues placement constraint was achieved after 6 iterations in the second phase of the synthesis procedure. The sub-optimal SOF controller K, determined using the algorithm presented above for the augmented dynamics P and for the forward speed of 2.0 m/s is

$$K = \begin{bmatrix} -0.0086 & -0.0366 & 0.0312 & -0.1820 & -0.4080 & 0.3053 & -2.1357 \\ 0.3311 & 1.4135 & -0.0638 & -0.3120 & 0.0337 & -0.6098 & 3.4339 \\ -0.0691 & -0.2782 & 0.0002 & 0.1116 & 1.7494 & -0.0065 & 0.6050 \\ -0.2687 & -1.1510 & 0.0011 & 0.4507 & 7.3011 & -0.0258 & 2.5146 \end{bmatrix}.$$

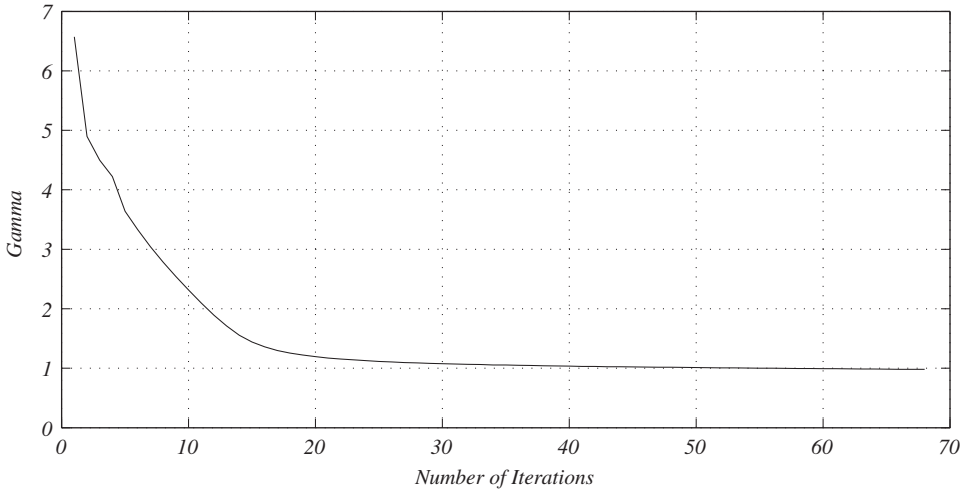

Fig. 9. Evolution of γ.

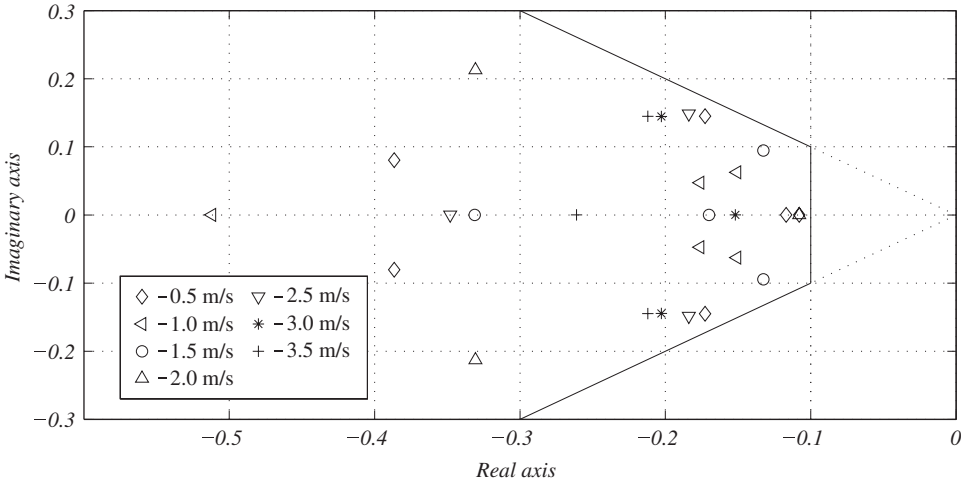

Fig. 10. Resulting closed-loop eigenvalues.

Fig. 10 displays the dominant closed-loop eigenvalues for the set of controllers synthesized for different vehicle speeds. In the figure the closed-loop eigenvalue regional placement constraint is represented by a solid line. It is evident that the constraint is satisfied by the different controllers synthesized for vehicle's speeds in the interval $[0.5, 3.5]$ m/s.

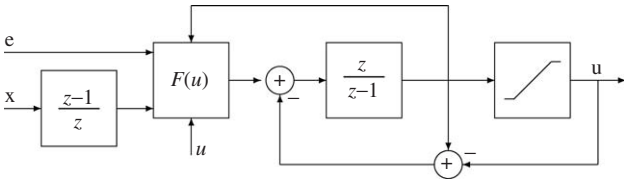

Fig. 11. *D* Controller implementation with anti-windup mechanism.

3.5. Non-linear controller implementation

A set of controllers was designed for a finite number of operating points, and their parameters interpolated according to the vehicle's forward speed (scheduling variable). The implementation of the resulting nonlinear gain-scheduled controller was done using the *D*-methodology described in Kaminer et al. (1995). This leads to the general structure for the implementation of discrete-time gain-scheduled controllers depicted in Fig. 11, where $F(u)$ denotes the block that interpolates the reduced order output feedback controllers obtained from the discretization of the linear controller designs in Section 3.3. The feedback chain from the integrators output to the block $F(u)$ implements the "washout" for the bow plane channel. In the present case a sampling frequency of 10 Hz was selected. In the figure, $\mathbf{u} = [\delta_b, \delta_s]'$ is vector of the bow and stern planes deflection, $\mathbf{e} = z_e$ is the depth tracking error and $\mathbf{x} = [q, z, \theta]'$. The limits on the saturation block were set to $+30^\circ$ and -30°, to prevent plane stalling. Notice that at trimming, the variable $\mathbf{e} = z_e$ and the vector at the output of the discrete "differentiator" are both zero. As explained in Kaminer et al. (1995) for the continuous time

setup, this simple but important fact is the reason why the linearization of the nonlinear gain scheduled system about an equilibrium condition will not introduce any extra terms arising from the additional feedback loop u, thus recovering the properties of the linear designs. Furthermore, it avoids feedforwarding the trimming values for the inputs and state variables.

4. Tests at sea

To assess the performance of the controller developed, a series of tests were carried out at sea. The vehicle was operated at constant heading and low depths, under the influence of strong wave action. Figs. 12–15 show some of the practical results obtained during depth changing maneuvers, together with the results of simulations obtained with a full nonlinear model of the vehicle. At the beginning of this maneuver INFANTE was at surface; 20 s into the maneuver the depth controller was switched on and a command to dive to 8 m depth was applied; this was followed by a command to dive to 10 m at $t = 150$ s. In the figures, the dashed and solid lines represent the experimental and the simulation results, respectively. The vehicle's forward speed was kept approximately constant at 1.8 m/s.

Figs. 12–14 show commanded and measured depth, pitch and pitch rate activity, respectively. Fig. 15 displays the activity of the bow planes. Notice the strong coupling between wave action and control planes deflection near the surface, mainly induced by pitch and pitch rate. Leaving aside the influence of the waves (which was not addressed explicitly in the controller design phase), the figures reveal close agreement between predicted and actual maneuvers.

5. Conclusions

The paper described the design and experimental testing of a control system for the INFANTE AUV in the vertical plane. The general setup adopted for controller design was nonlinear gain-scheduling control, whereby a set of *linear*

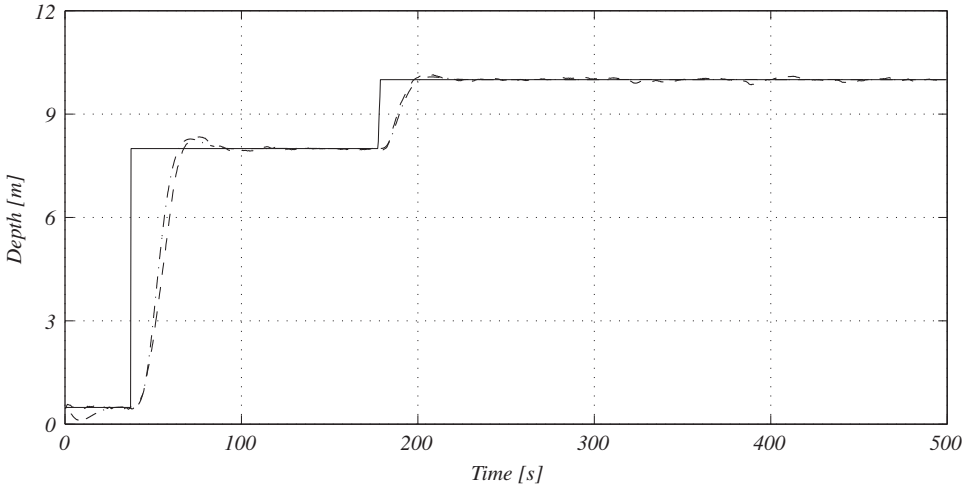

Fig. 12. Commanded and measured depth—simulated and measured values.

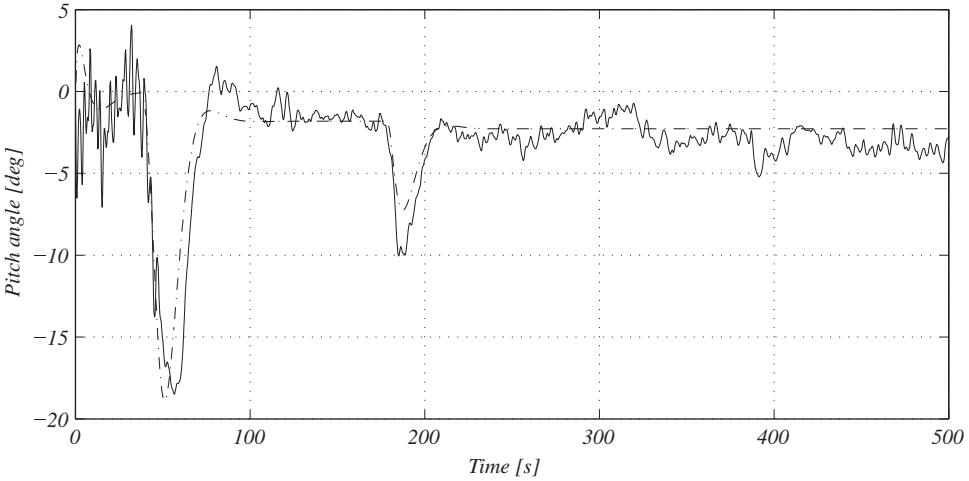

Fig. 13. Pitch angle—simulated and measured values.

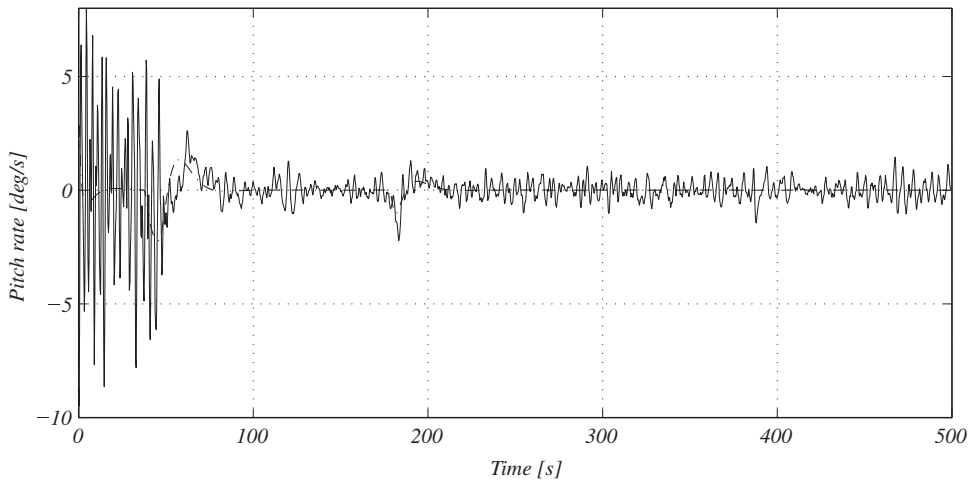

Fig. 14. Pitch rate—simulated and measured values.

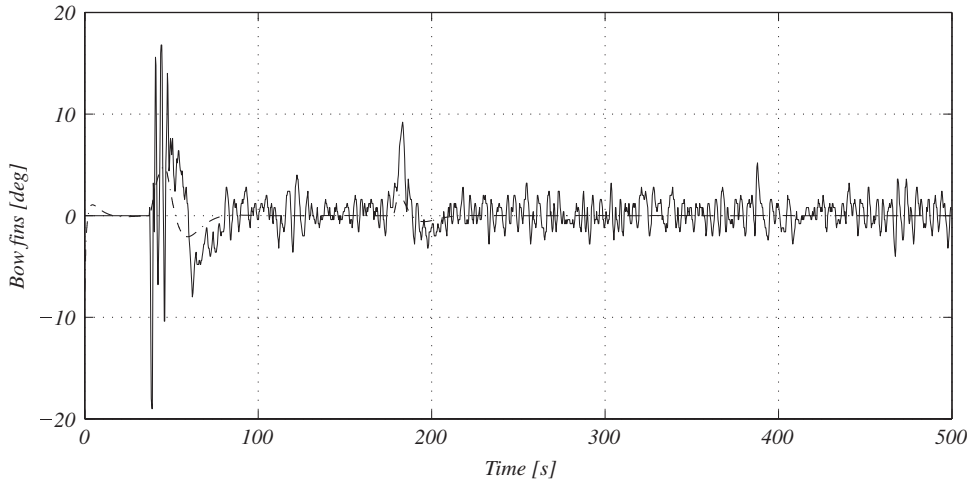

Fig. 15. Bow plane deflection under strong wave action.

finite reduced order output feedback controllers were designed using linear matrix inequality (LMI) based techniques. The methodology adopted addressed explicitly the fact that one of the vehicle states is not easily accessible for measurement. Furthermore, it is well rooted in recent theoretical advances in control theory and numerical analysis. The performance of the controller developed was evaluated using the proposed methodology was evaluated during tests at sea. The controllers implemented have proven extremely reliable over a long series of missions with the INFANTE AUV. Further problems that warrant further research include AUV control close to the surface in the presence of strong wave action and AUV terrain following.

Acknowledgments

The authors would like to thank to João Alves, Luis Sebastião, Manuel Rufino and Rudolfo Oliveira from ISR/IST for their valuable contribution to the development and testing of the INFANTE vehicle.

References

Abkowitz, M. (1964). *Lectures on ship hydrodynamics—steering and maneuverability*. Technical Report Hy-5, Technical University of Denmark, Hydrodynamics Department, Lyngby, Denmark, May 1964.

Apkarian, P., & Noll, D. (2006). Nonsmooth $\mathbf{H}_\infty$ Synthesis. *IEEE Transactions on Automatic Control*, *51*(1), 71–86.

Bara, G. I., & Boutayeb, M. (2005). Static output feedback stabilization with $\mathbf{H}_\infty$ performance for linear discrete-time systems. *IEEE Transactions on Automatic Control*, *50*(2), 250–254.

Benton, R. E., Jr., & Smith, D. (2005). A static-output-feedback design procedure for robust emergency lateral control of a highway vehicle. *IEEE Transactions Control Systems Technology*, *13*(4), 618–623.

Boyd, S., El Ghaoui, Feron, E., & Balakrishnan, V. (1994). *Linear Matrix Inequalities in System and Control Theory*. SIAM, Philadelphia, USA: Society for Industrial and Applied Mathematics.

Chilali, M., & Gahinet, P. (1996). $\mathbf{H}_\infty$ design with pole placement constraints: An LMI approach. *IEEE Transactions on Automatic Control*, *41*(3), 358–367.

Egeskov, P., Bjerrum, A., Pascoal, A., Silvestre, C., Aage, C., & Wagner Smitt, L. (1994). Design, construction and hydrodynamic testing of the AUV MARIUS. In *Proceedings of the AUV 94*, Cambridge, MA, USA.

El Ghaoui, L., & Niculescu, S. I. (1999) (Eds.). *Advances in linear matrix inequality methods in control*. Society for Industrial and Applied Mathematics, Philadelphia: SIAM.

El Ghaoui, L., Oustry, F., & AitRami, M. (1997). A cone complementary linearization algorithm for static output-feedback and related problems. *IEEE Transactions on Automatic Control*, *42*(8), 1171–1176.

Fossen, T. (1994). *Guidance and control of ocean vehicles*. Wiley.

Grigoriadis, K. M., & Skelton, R. E. (1996). Low order control design for LMI problems using alternating projection methods. *Automatica*, *32*, 1117–1125.

Harvald, Sv. Aa. (1983). *Resistance and propulsion of ships*. New York, USA: Wiley.

Henrion, D., & Lasserre, J. B. (2006). Convergent relaxations of polynomial matrix inequalities and static output feedback. *IEEE Transactions on Automatic Control*, *51*(1), 192–202.

Iwasaki, T., Skelton, R., & Geromel, J. (1994). Linear quadratic suboptimal control with static output feedback. *Systems and Control Letters*, *32*(6), 421–430.

Kaminer, I., Pascoal, A., Khargonekar, P., & Coleman, E. (1995). A velocity algorithm for the implementation of gain-scheduled controllers. *Automatica*, *31*, 1185–1191.

Kharitonov, V. L., Niculescu, S. I., Moreno, J., & Michiels, W. (2005). Static output feedback stabilization: Necessary conditions for multiple delay controllers. *IEEE Transactions on Automatic Control*, *50*(1), 82–86.

Lamb, H. (1932). *Hydrodynamics*. New York, USA: Cambridge.

Leibfritz, F. (2001). An LMI-based Algorithm for designing suboptimal static output feedback controllers. *SIAM Journal on Control and Optimization*, *39*(6), 1711–1735.

Lewis E. V. (1990) (Ed.). *Principles of naval architecture*. Jersey City, USA: The Society of Naval and Marine Engineers.

Mäkilä, P. M. (1985). Parametric LQ control. *International Journal of Control*, *41*(6), 1413–1428.

Newman, J. N. (1977). *Marine hydrodynamics*. Cambridge, MA, USA: The MIT Press.

Rugh, W., & Shamma, J. S. (2000). A survey of research on gain-scheduling. *Automatica*, 261–268.

Silvestre, C. (2000). *Multi-objective optimization theory with applications to the integrated design of controllers/plants for autonomous vehicles*. Ph.D. thesis, Department of Electrical Engineering and Computer Science, Instituto Superior Técnico, Lisbon, Portugal.

Zhou, K., Doyle, J. C., & Glover, K. (1995). *Robust and optimal control*. New Jersey, USA: Prentice-Hall.